Atmospheric Research 164–165 (2015) 347–357

Contents lists available at ScienceDirect

Atmospheric Research

journal homepage: www.elsevier.com/locate/atmos

Global modeling of the nitrate radical (NO_3) for present and pre-industrial scenarios

M.A.H. Khan [a], M.C. Cooke [a,1], S.R. Utembe [a,2], A.T. Archibald [a,3], R.G. Derwent [b], P. Xiao [a], C.J. Percival [c], M.E. Jenkin [d], W.C. Morris [a], D.E. Shallcross [a,*]

[a] Biogeochemistry Research Centre, School of Chemistry, University of Bristol, Cantock's Close, Bristol BS8 1TS, UK
[b] rdscientific, Newbury, Berkshire, UK
[c] The Centre for Atmospheric Science, The School of Earth, Atmospheric and Environmental Science, The University of Manchester, Simon Building, Brunswick Street, Manchester, M13 9PL, UK
[d] Atmospheric Chemistry Services, Okehampton, Devon, EX20 4QB, UK

ARTICLE INFO

Article history:
Received 23 February 2015
Received in revised form 26 May 2015
Accepted 8 June 2015
Available online 14 June 2015

Keywords:
STOCHEM-CRI
NO_3
HO_x recycling
Pre-industrial scenario
Present scenario

ABSTRACT

Increasing the complexity of the chemistry scheme in the global chemistry transport model STOCHEM to STOCHEM-CRI (Utembe et al., 2010) leads to an increase in NO_x as well as ozone resulting in higher NO_3 production over forested regions and regions impacted by anthropogenic emission. Peak NO_3 is located over the continents near NO_x emission sources. NO_3 is formed in the main by the reaction of NO_2 with O_3, and the significant losses of NO_3 are due to the photolysis and the reactions with NO and VOCs. Isoprene is an important biogenic VOC, and the possibility of HO_x recycling via isoprene chemistry and other mechanisms such as the reaction of RO_2 with HO_2 has been investigated previously (Archibald et al., 2010a). The importance of including HO_x recycling processes on the global budget of NO_3 for present and pre-industrial scenarios has been studied using STOCHEM-CRI, and the results are compared. The large increase (up to 60% for present and up to 80% for pre-industrial) in NO_3 is driven by the reduced lifetime of emitted VOCs because of the increase in the HO_x concentration. The maximum concentration changes (up to 15 ppt) for NO_3 from pre-industrial to present day are found at the surface between 30°N and 60°N because of the increase in NO_x concentrations in the present day integrations.

1. Introduction

The nitrate radical (NO_3) is the dominant night-time oxidant in the atmosphere (e.g. Geyer et al., 2001a; Platt et al., 2002; Wayne et al., 1991), but because of its low concentration and rapid photolysis, it is less important during the daytime. Significant levels (typically pptv) of NO_3 have been detected over a wide range of atmospheric conditions, indicating a potential role for NO_3 in oxidation chemistry over large regions of the atmosphere (e.g. Wayne et al., 1991; Brown and Stutz, 2012). The importance of the nitrate radical as a night-time oxidant has stimulated many studies to investigate the reaction rates and mechanisms involved (e.g. Wayne et al., 1991; Atkinson and Arey, 2003; Monks, 2005; Brown and Stutz, 2012). At night time, NO_3 reacts rapidly with a number of unsaturated hydrocarbons (Atkinson, 1991; Geyer et al., 2001a), thus impacting the budgets of these species and their degradation products. In the continental boundary layer over Europe, it was found that NO_3 contributed 28% to the overall VOC initiated oxidation over a 24 hour period (Geyer et al., 2001a).

NO_3 is predominantly formed by reaction of nitrogen dioxide (NO_2) with ozone (O_3).

$$NO_2 + O_3 \rightarrow NO_3 + O_2 \quad (1)$$

Stabilized Criegee Intermediates (SCI) formed from the ozonolysis of alkenes can react with NO_2 to produce NO_3 (Presto and Donahue, 2004; Welz et al., 2012; Ouyang et al., 2013) and could be a non-negligible source of NO_3, especially indoors (Shallcross et al., 2014; Taatjes et al., 2013). It has been shown that the generation of NO_3 via reactions (2) and (3) scales directly with level of alkene (Welz et al., 2012; Percival et al., 2013; Shallcross et al., 2014)

$$\text{Alkene} + O_3 \rightarrow \alpha\text{CI} + (1-\alpha)\text{SCI} + \text{carbonyl} \quad (2)$$

$$\text{SCI} + NO_2 \rightarrow NO_3 + \text{carbonyl} \quad (3)$$

The NO_3 accumulated during night time through reactions (1–3) can then react with NO_2 to form N_2O_5.

$$NO_2 + NO_3 + M \leftrightharpoons N_2O_5 + M \quad (4)$$

* Corresponding author. Tel.: +44 117 928 7796.
E-mail address: d.e.shallcross@bristol.ac.uk (D.E. Shallcross).
[1] Now at the Met Office, FitzRoy Road, Exeter, Devon, EX1 3PB, UK.
[2] Now at the School of Earth Sciences, University of Melbourne, Parkville VIC 3010, Australia.
[3] Now at the Centre for Atmospheric Science, University of Cambridge, Cambridge, UK.

http://dx.doi.org/10.1016/j.atmosres.2015.06.006

N_2O_5 can thermally dissociate to release and transport NO_3 away from the source region. The timescale for the thermal equilibrium of NO_2, NO_3, and N_2O_5 is of the order of minutes in the boundary layer, favoring N_2O_5 at lower temperature and moderately polluted conditions.

N_2O_5 can be lost to surfaces with uptake coefficients in the range of 0.001–0.05 (Hallquist et al., 2000; Kane et al., 2001; Brown et al., 2006). N_2O_5 can react heterogeneously on aerosols and cloud particles and homogeneously with water to yield HNO_3 (Heintz et al., 1996; Wayne et al., 1991).

$$N_2O_5 + H_2O \rightarrow 2HNO_3 \quad (5)$$

During the day time, NO_3 is destroyed primarily by rapid photolysis, having a lifetime of only 5 s for overhead sun and clear sky conditions (Orlando et al., 1993; Monks, 2005).

$$NO_3 + h\nu \rightarrow NO + O_2 \quad (6a)$$

$$NO_3 + h\nu \rightarrow NO_2 + O(^3P) \quad (6b)$$

Under highly polluted conditions, NO_3 can persist during the day and contribute significantly to the oxidation of certain VOCs (e.g. α-pinene, p-cresol, and other terpenes) (Geyer et al., 2003).

In areas with large NO emissions, the influence on the level of NO_3 can be significant by reacting rapidly with NO (e.g. Brown et al., 2005; Khan et al., 2008).

$$NO_3 + NO \rightarrow NO_2 + NO_2 \quad (7)$$

NO_3 can produce OH directly through reaction with HO_2 (e.g. Hall et al., 1988; Mellouki et al., 1993)

$$NO_3 + HO_2 \rightarrow NO_2 + OH + O_2 \quad (8)$$

and indirectly through the production of HO_2 and aldehydes ($R_{-H}O$) following reaction with peroxy radicals (RO_2), depicted by the overall reaction (Biggs et al., 1994, 1995; Crowley et al., 1990; Daele et al., 1995; Kukui et al., 1995; Ray et al., 1996; Canosa-Mas et al., 1996; Vaughan et al., 2006; Stone et al., 2014).

$$NO_3 + RO_2 \rightarrow NO_2 + R_{-H}O + HO_2 \quad (9)$$

The NO_3 radical is highly reactive towards some unsaturated hydrocarbons and most importantly isoprene and terpenes, leading to the production of peroxy radicals at night (Platt et al., 1990).

The lifetime of NO_3 is very short with respect to the loss processes (see Appendix A for the typical values). NO_3 also reacts rapidly with dimethylsulphide (DMS), which is potentially significant in the marine boundary layer (Heintz et al., 1996). Previous studies suggested that NO_3 chemistry dominates the oxidation of DMS in coastal areas (Yvon et al., 1996; Allan et al., 1999; Stark et al., 2007) and that globally 24% of DMS is oxidized via reaction with NO_3 (Breider et al., 2010). If the concentration of NO_2 is 60% higher than that of DMS, NO_3 acts as a more important oxidant than OH for DMS in the marine boundary layer (Allan et al., 2000). The reaction of NO_3 with hydrocarbons (e.g. isoprene and terpenes) can lead to the formation of secondary organic aerosol (SOA). The SOA yield of the reaction between NO_3 and isoprene is 4.3–23.8% in terms of organic mass (Ng et al., 2008).

Several field measurements of NO_3 have been conducted using differential optical absorption spectroscopy (DOAS) in a long path through the atmosphere (Aliwell and Jones, 1996; Platt et al., 1980; Geyer et al., 2001a), cavity ring down spectroscopy (CRDS) (King et al, 2000; Brown et al., 2001, 2002; Ball et al., 2001), laser-induced fluorescence (LIF) (Wood et al., 2003; Matsumoto et al., 2005), and electron spin resonance spectroscopy (ESR) (Mihelcic et al., 1993). However, field studies measuring NO_3 are limited and most NO_3 measurements were taken over highly polluted cities. In general, model studies underestimate NO_3 concentration in comparison with field measurements (Mihelcic et al., 1993; Sommariva et al., 2007) indicating perhaps missing nighttime NO_3 oxidation processes.

The impact of NO_3 chemistry on the removal of hydrocarbons, O_3, and NO_x at night on regional to global scales and throughout the year is not constrained well. A knowledge and understanding of the concentration and distribution of NO_3 is essential to evaluate properly the concentration of organic species in the atmosphere. For example, addition of NO_3 to an alkene could result in direct production of an organic nitrate, whereas via OH initiated chemistry, first the OH must add to the alkene to form a hydroxyl-peroxy species, and then this peroxy radical must react with NO via the minor channel to form a hydroxyl-nitrate. In this study, the global budget and the global distribution of NO_3 has been presented using the STOCHEM-CRI global chemistry transport model. The effects of including HO_x recycling (Archibald et al., 2010a) in the global model of NO_3 for the present and pre-industrial scenario are evaluated in this study.

2. Model description

2.1. Global chemistry transport model studies

The global chemistry transport model, STOCHEM, used in this study is a 3-dimensional chemical transport model (CTM) in which 50,000 constant mass air parcels are advected every 3 hours by wind from the Meteorological Office Hadley Centre general circulation model (GCM) using a Lagrangian approach allowing the chemistry and transport processes to be uncoupled. The Lagrangian cells are based on a grid of 1.25° longitude, 0.8333° latitude, and 12 unevenly spaced (with respect to altitude) vertical levels with an upper boundary of 100 hPa (Collins et al., 1997). The detailed description of the vertical levels and advection scheme used in STOCHEM can be found in Appendix B. The chemical mechanism used in STOCHEM, is the common representative intermediates mechanism version 2 and reduction 5 (CRI v2-R5), referred to as 'STOCHEM-CRI'. The detail of the CRI v2-R5 mechanism is given by Jenkin et al. (2008), Watson et al. (2008), and Utembe et al. (2009) with updates highlighted in Utembe et al. (2010). The mechanism consists of 27 emitted non-methane hydrocarbons and 229 chemical species which take part in 627 reactions. The emissions data employed in the base case STOCHEM model were adapted from the Precursor of Ozone and their Effects in the Troposphere (POET) inventory (Granier et al., 2005) for the year 1998. Emission totals for CH_4 were taken from the inverse model study of Mikaloff-Fletcher et al. (2004), except for the ocean emission which was from Houweling et al. (2000). The anthropogenic and biomass burning emissions of the aromatic species o-xylene, benzene, and toluene were taken from Henze et al. (2008). Biomass burning emissions of ethyne, formaldehyde and acetic acid were produced using scaling factors from Andreae and Merlet (2001) per mole CO emitted.

In a recent study of Archibald et al. (2010b), a box model was employed using the MCM v3.1 as a reference benchmark, and sensitivity studies were performed to investigate the effects of recent mechanistic changes to our understanding of isoprene photochemistry on the HO_x budget. More details about isoprene mechanism used in STOCHEM-CRI can be found in Appendix C. Two experiments were conducted to investigate the global impacts of mechanistic changes for CRI v2-R5. The present day results compare the base case reference run referred to as 'Base' described in Utembe et al. (2010) with a model including the isoprene HO_x recycling referred to as 'ISOP' described in Archibald et al. (2010a). Two further integrations (referred to as 'B1800' and 'ISOP1800') were performed for a pre-industrial scenario where anthropogenic emissions were completely removed from the model and the biomass burning emissions were reduced with the aim to remove the majority of human-induced effects. Global gridded emissions of CH_4, CO, CO_2, SO_2, N_2O, NO_x, NH_3, and non-methane volatile organic compounds by sector for the period of 1890–1990 were estimated by van

Aardenne et al. (2001). This emissions dataset, EDGAR-HYDE was estimated using historical activity data from the HYDE database (Klein Goldewijk and Battjes, 1997) and historical emission sources based on the emission factors for uncontrolled sources in EDGAR 2.0 for 1990. The biomass burning emissions used in this study have been scaled using global scaling factors from the Edgar-Hyde emissions database (1890–1990). The scaling factors were produced by calculating global ratios between 1890 and the present day for each species and scaling the base-case emissions for 1800 by these factors. Global scaling factors were applied to the initialization of the model runs based on the global totals in Table 1. The pre-industrial scenario is designed to be representative of the Earth's atmosphere without human-induced effects. The same meteorology was used in the pre-industrial simulation and thus this study is only based on the emission changes and no consideration was taken into account for changes in climate. In order to investigate the effect of human activity, emissions from vegetation, soil, and oceans are the same for all simulations. Vegetation changes since pre-industrial are expected to be only 2–3% (Lathiere et al., 2005). This is an oversimplification but allows for effects of human activity to be investigated in isolation and is consistent with the approach of other studies (Hoyle et al., 2009; Tsigaridis et al., 2006). All simulations were conducted with meteorology from 1998 for a period of 24 months with the first 12 allowing the model to spin up. Analysis is performed on the subsequent 12 months of data.

3. Results and discussion

3.1. $NO_3 + N_2O_5$ budget

Table 2 shows the $NO_3 + N_2O_5$ (referred as NO_{3s} family) budget (in percentage terms) produced by the STOCHEM-CRI model for both present and pre-industrial scenarios. The production of NO_{3s} occurs almost entirely through the formation of NO_3 by the reaction of NO_2 with O_3 (96% for pre-industrial and 98% for present case), with an additional production from the reaction of OH + HNO_3 (4% for pre-industrial and 2% for present case). The main sink of NO_{3s} is due to NO_3 loss by photolysis (39% for pre-industrial and 36% for present case). Additional significant loss processes of NO_{3s} are due to the reaction with NO (9% for pre-industrial and 18% for present case), with DMS (5% for pre-industrial and 3% for present case), with HO_2 (6% for pre-industrial and 7% for present case), with oxidation products of VOCs (e.g. CH_3O_2 and CH_3CO_3) (11% for both pre-industrial and present case), with isoprene and monoterpenes (20% for pre-industrial and 11% for present case). As a result of the significant increase in NO_x in the present day in comparison with a pre-industrial scenario, the loss term of NO_3 due to the reaction with NO is significantly enhanced and the loss by the reaction with VOC is decreased accordingly (See Table 2). The loss of N_2O_5 due to the reaction with H_2O vapor is found to be 2.6% and 5.0% for pre-industrial and present scenarios, respectively. A recent N_2O_5 heterogeneous chemistry parameterization (based on Bertram and Thornton, 2009) using the MOSAIC aerosol module coupled with the CRIv2-R5 and CBM-Z chemical schemes (Archer-Nicholls et al., 2014) shows that N_2O_5 heterogeneous chemistry can reduce significantly (up to 30%) the build-up of NO_3 throughout the night. In STOCHEM, it is assumed that the conversion of gaseous precursor to coarse mode aerosol occurs with a globally fixed time constant which has the order of magnitude of 2% per hour (Derwent et al., 2003), thus a large error associated with the calculation of heterogeneous loss of N_2O_5 in this study. However, applying the parameterization of Bertram and Thornton (2009) into STOCHEM could improve model representations of atmospheric global NO_3.

Table 1
Global emission breakdown by major group for the pre-industrial (1800) and present day simulations (1998).

Species	1800	1998
Nitrogen, Tg N yr^{-1}		
NO_x	21.1	56.7
NH_3	12.2	53.6
Total	**33.3**	**110.3**
Carbon, Tg C yr^{-1}		
CO	139.5	523.7
CH_4	253.8	461.3
Non methane VOC	675.1	789.4
Primary organic aerosol (POA)	17.6	58.9
Total	**1086.0**	**1833.3**
Sulfur, Tg S yr^{-1}		
SO_2	0.8	58.8
DMS	16.0	16.0
Total	**16.8**	**74.8**

Table 2
The main sources and sinks of NO_{3s} in STOCHEM-CRI, values are a percentage (%) of the global production and loss of NO_3 and N_2O_5. Minor reactions are grouped together as 'Others'.

Reaction	Pre-industrial		Present	
	B1800	ISOP1800	Base	ISOP
Sources				
$NO_2 + O_3 \rightarrow NO_3 + O_2$	95.7	95.0	97.6	97.3
$HNO_3 + OH \rightarrow NO_3 + H_2O$	4.3	5.0	2.4	2.7
Sinks				
$NO_3 + h\nu \rightarrow NO_2 + O$	33.5	33.2	31.4	31.3
$NO_3 + NO \rightarrow NO_2 + NO_2$	9.1	8.6	17.8	17.6
$NO_3 + C_5H_8 \rightarrow$ NRU14O2	11.7	11.9	6.4	6.2
$NO_3 + HO_2 \rightarrow NO_2 + OH + O_2$	5.6	5.9	7.0	7.3
$NO_3 + h\nu \rightarrow NO + O_2$	5.1	5.0	4.7	4.7
$NO_3 + \alpha$-pinene → NRTN28O2	5.6	6.2	2.9	3.1
$NO_3 + CH_3O_2 \rightarrow HO_2 + HCHO + NO_2$	8.0	7.7	8.1	8.0
$NO_3 + DMS \rightarrow CH_3SO + HCHO + HNO_3$	5.3	5.2	3.1	3.2
$NO_3 + CH_3CO_3 \rightarrow CH_3O_2 + NO_2$	3.3	3.0	3.2	2.9
$NO_3 + \beta$-pinene → NRTX28O2	2.4	2.5	1.4	1.5
$N_2O_5 \rightarrow HNO_3 + HNO_3$	2.6	2.8	5.0	5.2
Others	7.8	8.0	9.0	9.0

Notes: Closest MCM v3.2 analogs of NRU14O2, NRTN28O2, NRTX28O2 are NISOPO2, (NAPINAO2 + NAPINBO2), (NBPINAO2 + NBPINBO2), respectively. Structures of these species can be obtained using species name and search facility on MCM website (http://mcm.leeds.ac.uk/MCM/search.htt).

3.2. Comparison of the model predictions with NO_3 observations

Measuring vertical profiles of NO_3 is critical since it is present predominantly at night when the boundary layer is shallow and poorly mixed. Brown et al. (2007) used a cavity ring down based spectrometer to measure night-time NO_3 profiles during the 2004 New England Air Quality Study (NEAQS) over North America. Measured values of NO_3 were at a maximum at about 0.5 km with night-time mean values between 20 pptv and 90 pptv. There was also a considerable concentration above the nocturnal boundary layer with night-time values up to 20 pptv reported at 1.5 km (Brown et al., 2007). The annual mean night-time values in the surface layer over the northeastern seaboard of the USA are estimated in our model to be 10–25 pptv. The surface level measurements alone cannot present a complete picture of night-time NO_3 chemistry (e.g. Fish et al., 1999; Galmarini et al., 1997). The comparison of globally modeled NO_3 with *in situ* measurements is difficult because of the short lifetime of NO_3 and the location of the measurement sites. Most short-term NO_3 measurements were performed over highly polluted cities, and night-time values of more than 800 pptv have been reported by Asaf et al. (2009). It is not reasonable to expect a background CTM to capture urban levels of NO_3 because the observed NO_3 values may not represent the average state of the region due to the unusual meteorology and the coarse emission grids in STOCHEM make it difficult to evaluate model NO_3 levels in the sites near strong source regions. However, we compare a range of different geographical (e.g. Continental Boundary Layer, Marine Boundary

Table 3
Comparison of observed NO_3 mixing ratios (pptv) in different environments with our model results, CBL: Continental Boundary Layer; MBL: Marine Boundary Layer. The standard errors (absorption cross-sections, systematic) of DOAS ranged between 10% and 20%, the variation of the LIF's sensitivity is ± 17%, and the uncertainties of the ESR and CRD are ± 5% and ± 15%, respectively.

Location	Time	Environmental	Measurement type and detection limit (ppt)	Observed (ppt)	Model Base (ppt)
Geyer et al. (2001b) Lindenberg, Germany (52°N, 14°E)	Feb–Sep 1998	Rural, CBL	DOAS, 3.4	4.6	6.9
Crowley et al. (2010) Taunus Observatory, Germany (50°N, 8°E)	May 2008	Rural, CBL	CRDS, 1	20–40	6.9
Asaf et al. (2010) Jerusalem, Palestine (32°N, 35°E)	Jul 2005 to Sep 2007	Urban, CBL	DOAS, 8.5	27.3 ± 43.5	9.2
Stutz et al. (2010) Houston, US (30°N, 95°W)	Aug–Sep 2006	Urban, CBL	DOAS, 3	0–149	3.3
Wang et al. (2013) Shanghai, China (31°N, 122°E)	Aug–Oct 2011	Urban, CBL	DOAS, 8	16.0 ± 9.0	16.6
Li et al. (2012) Guangzhou, China (23°N, 113°E)	Jul 2006	Rural, CBL	DOAS, 3.6	21.8 ± 1.8	4.7
Matsumoto et al. (2010) Izu-Oshima, Japan (35°N, 139°E)	June 2004	Clean, MBL	LIF, 10	3	4.4
Allan et al. (2000) Mace Head, Ireland (53 °N, 10°W)	July–Aug 1996 April–July 1997	Clean, MBL	DOAS, 0.6	5	3.8
Carslaw et al. (1997) Canary Island (28°N, 16°W)	May 1994	Clean, MBL	DOAS, 0.5	8.0 ± 3.0	5.0
Vrekoussis et al. (2007) Finokalia, Greece (35°N, 25°E)	Jun 2001 to Sep 2003	Coastline, MBL	DOAS, 1.2	4.2 ± 2.3	16.0
Allan et al. (1999) Weybourne, England (53°N, 1.8°E)	Oct–Nov 1994 June 1995	Semi-polluted, MBL	DOAS, 1.5	10 6	5.0 5.5
McLaren et al. (2010) East point, Canada (49°N, 123°W)	July–Aug 2005	Polluted, MBL	DOAS, 4.0	13.1	1.6
Mihelcic et al. (1993) Schauinsland, Germany (48°N, 8°E)	August 1990	Urban, CBL	ESR, 3.0	5.8	12.0

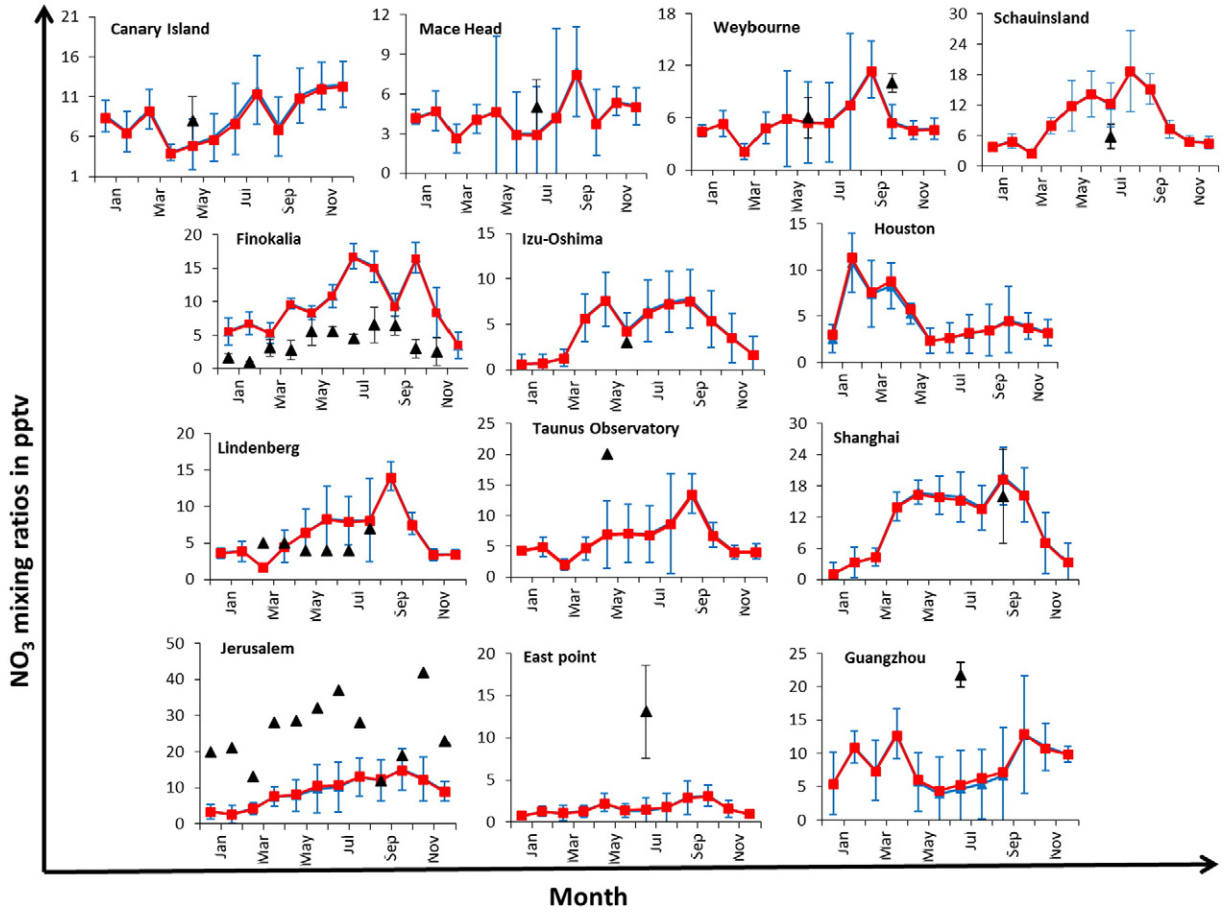

Fig. 1. Monthly variation of surface global NO_3 concentration of selected monitoring stations produced by the STOCHEM-CRI; the blue line represents base run, the red line represents HO_x recycling run, the black triangle symbols represent the measurement data, black error bars represent measurement variability, and the blue error bars represent model error based on errors in sources and sinks.

Layer) and environmental (e.g. urban, rural, semi-polluted, polluted, and clean) measurement data with our model results (Table 3). The field campaign results gave higher NO_3 concentrations than the model. Daytime NO_3 has a very short lifetime of only 5 s, so comparing monthly averaged model NO_3 with measurements predominantly during the night is not robust. Direct comparison between model and measurement is difficult due to the model uncertainties associated with the chemistry, meteorology, and emission scenarios. The meteorological data that drive the model at present are derived from the year 1998, and therefore, when comparing with measurement data from other years, the inter-annual variation must be taken into account.

The average monthly variation of surface global NO_3 mixing ratios (for both base and HO_x recycling cases) and NO_2 and O_3 mixing ratios (for base case) for selected monitoring stations produced by the STOCHEM-CRI are presented in Figs. 1 and 2, respectively. The model results are then compared with the field measurement data shown in Figs. 1 and 2. The modeled data showed that higher levels of NO_3 prevail in summer and lower concentrations are present in the winter months for most of the surface stations. The higher temperatures and high level of O_3 in summer time (see Fig. 2) allow NO_3 to be produced more rapidly from the oxidation of NO_2 by O_3 together with the fact that k_1 is highly temperature dependent. The inclusion of HO_x recycling leads to a slight increase in NO_3 levels in the urban CBL and polluted MBL, no significant change in the rural CBL, whilst a slight decrease in NO_3 levels in the clean MBL is observed.

Lindenberg, Schauinsland, and Taunus Observatory are surface stations in Germany and all locations are surrounded by forests. There is a large variation in the measured NO_3 mixing ratios at German stations with a maximum recorded value of 40 pptv at the Taunus Observatory because the Lindenberg and Schauinsland sites have no significant anthropogenic emissions and the Taunus Observatory has received pollution from nearby urban centers and traffic. Our model results for these sites are close to the non-polluted measurement sites, Lindenberg (4.6 pptv) and Schauinsland (5.8 pptv). The measured concentration in the urban continental boundary layer for NO_3 at different surface stations (e.g. Jerusalem, Houston, Shanghai) varies significantly because of the different pollution events associated with different urban CBL stations at the time of measurements. The comparison between measured and modeled NO_3 concentrations for these stations highlights the difficulty of comparing CBL measured data with our model data. However, the modeled value (16.6 pptv) for Shanghai, China, matches with the measured value (16 pptv), whereas the modeled value (4.7 pptv) for Guangzhou, China, is much lower than the measured value (21.8 pptv). The large variation in the modeled NO_3 concentrations with respect to the measured NO_3 concentrations are found in China stations because of the difference of model NO_2 in Shanghai (2.2 ppb) and Guangzhou (0.8 ppb) compared with measured NO_2 in Shanghai (16 ppbv) and Guangzhou (18 ppbv) (Fig. 2). A recent study (Wang et al., 2014) found very high daytime $N_2O_5 + NO_3$ mixing ratios in the range of 200–1000 ppt at an urban site of Hong Kong, which is much higher than our model study. Chemical interferences in the thermal dissociation chemical ionization mass spectrometer (TD-CIMS) could have contributed most of the average daytime $N_2O_5 + NO_3$ in their study, but the elevated daytime $N_2O_5 + NO_3$ might be in part due to real contribution from NO_3 or N_2O_5. The stations in Izu-Oshima, Mace Head, and Canary Island are situated in the clean marine boundary layer. The modeled values at these stations fall within the range measured by Allan et al. (2000), Carslaw et al. (1997), and Matsumoto et al. (2010). Allan et al. (1999) reported a seasonal measurement of NO_3 at the Weybourne observatory on the east coast of England with

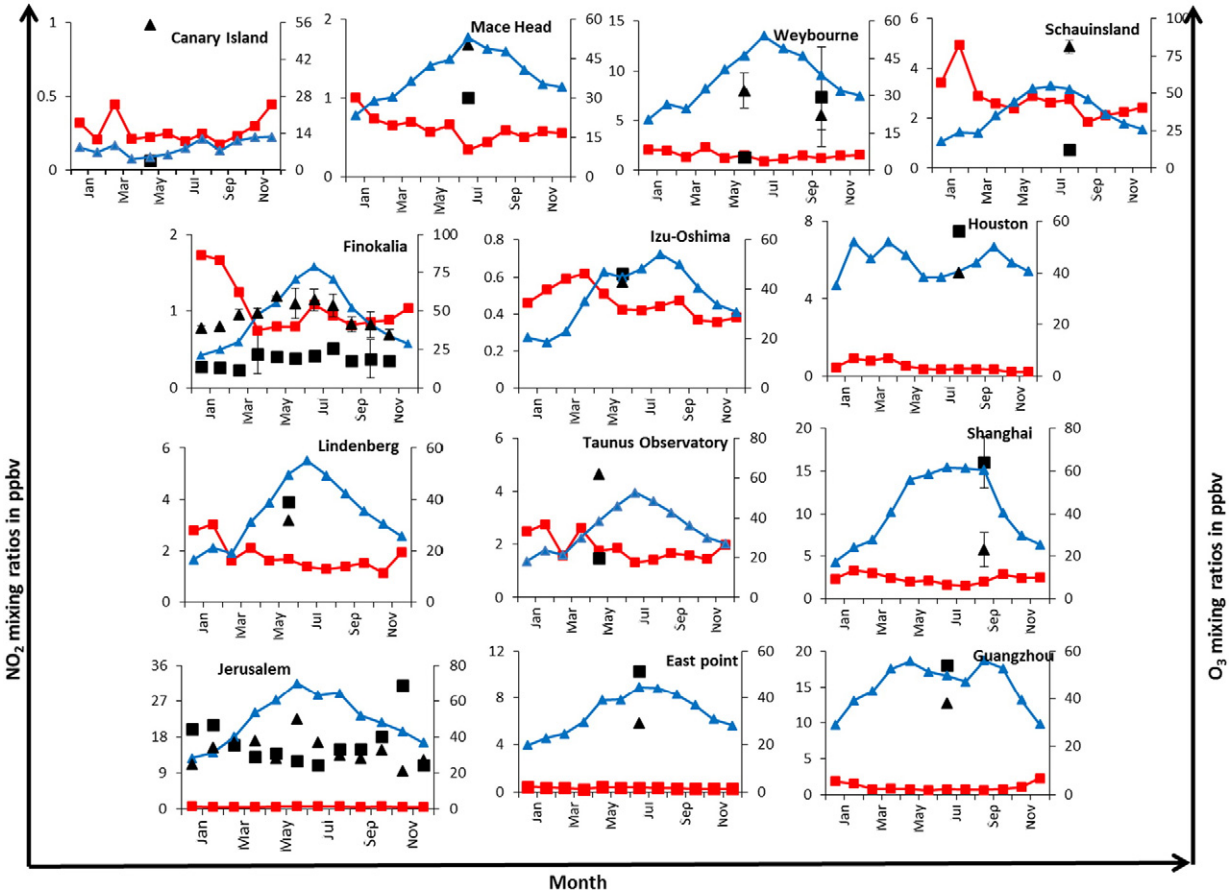

Fig. 2. Monthly variation of surface global NO_2 (red square symbols) and O_3 (blue triangle symbols) mixing ratios of selected monitoring stations produced by the STOCHEM-CRI, black square and triangle symbols represent the measurement data of NO_2 and O_3, respectively, and the black error bars represent measurement variability.

the reported values of 10 and 6 pptv for winter (semi-polluted air) and summer (clean air), respectively. Our modeled values are found to be 5.0 and 5.5 pptv in winter and summer, respectively. Analysis of the non-methane hydrocarbon database accumulated during the HANSA project (Penkett et al., 2007) showed higher NO_3 levels at the Weybourne observatory and an associated high oxidation efficiency. They concluded that NO_3 chemistry significantly modifies the average concentration of peroxy radicals and thus their precursor alkenes, predominantly during the winter month. Vrekoussis et al. (2007) reported NO_3 mixing ratios at a coastal MBL site, Finokalia ranged from 1 pptv to 38 pptv and averaged 4.2 pptv, with the highest levels found in polluted air masses transported from Greece, Turkey, and Central Europe. Our model result for this coastal site is found to be surprisingly high (16 pptv) because of high model NO_2 (see Fig. 2). A rural MBL in East point, Canada is heavily polluted by few direct anthropogenic sources (e.g. marine vessel traffic), leading to a higher level of NO_2 emission (McLaren et al., 2010). The measurement value of NO_3 (13.1 pptv) for this site was found to be much higher than our model value (1.6 pptv) because the higher NO_2 levels in this region (see Fig. 2) would increase the production rate of NO_3 via reaction (1).

The low resolution of the emission grids of our model (5° latitude × 5° longitude) compared with other global models (typically 1° latitude × 1° longitude) prevent regions of very low and very high NO_3 concentrations being investigated. Improving its resolution would allow an accurate comparison between modeled and measurement data to be conducted. However, the results indicate no immediate systematic biases or deficiencies in the NO_3 simulation.

3.3. Surface distribution of NO_3

Fig. 3 shows the surface distribution of NO_3 in December–January–February (D-J-F) and June–July–August (J-J-A) for both present and pre-industrial scenarios. The seasonal surface distribution of NO_3 is driven by the location of NO_x, O_3, and VOC emissions. Biomass burning

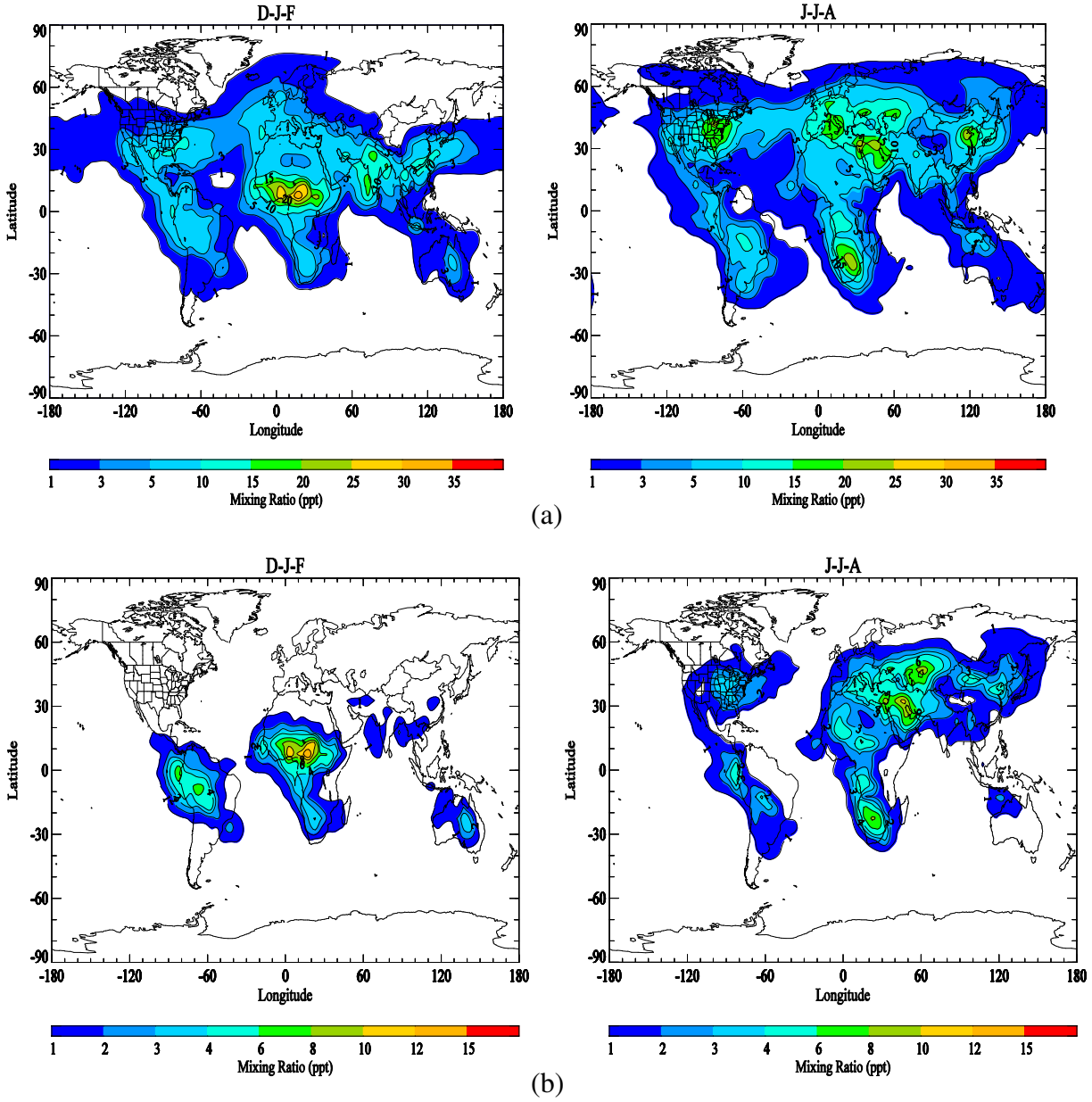

Fig. 3. Surface distribution of June–July–August and December–January–February time NO3 level simulated by the STOCHEM-CRI for (a) present and (b) pre-industrial scenarios.

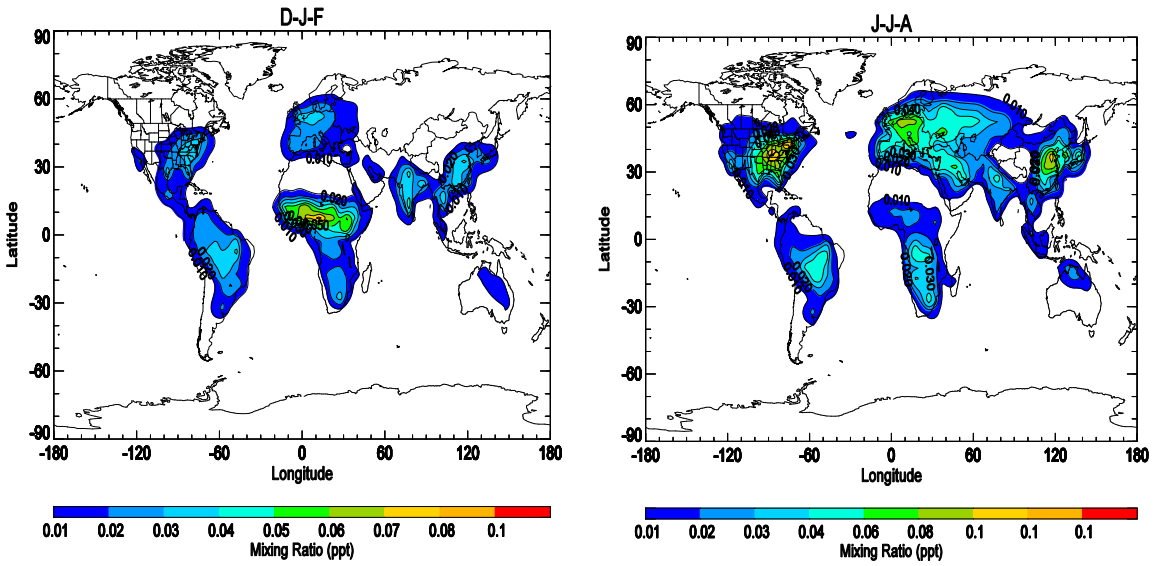

Fig. 4. Surface distribution of NO_3 produced through the reaction of NO_2 and O_3 simulated for present scenario.

and vegetative emissions are located in forested regions and anthropogenic emissions are predominantly distributed over North America, Central Europe, and South East Asia. In D-J-F time, the peak NO_3 was found in forested regions where emissions of NO_x and VOCs are large. The anthropogenic NO_x emissions are generally in between 30°N and 60°N, which in winter time has relatively slow photochemistry and thus levels of ozone are lower resulting in lower levels of NO_3 than over forested regions near the equator (See Fig. 3). In J-J-A time, the peak NO_3 was found over biomass burning regions of southern Africa and South America and anthropogenic emissions regions. Southern Africa and South America are near large VOC sources of isoprene and terpenes. In summer time, photochemistry between 30°N and 60°N is

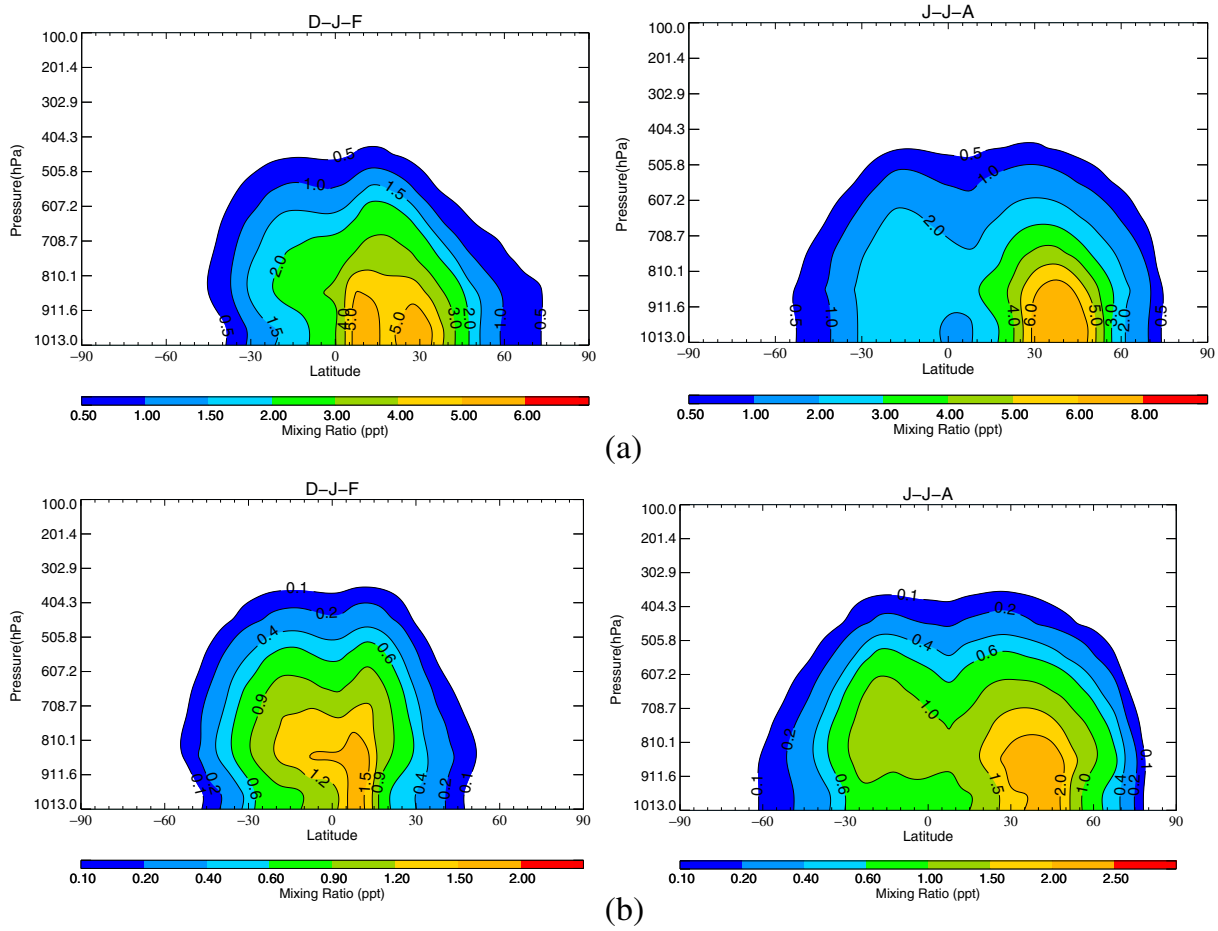

Fig 5. Annual mean zonal distribution of NO_3 simulated by the STOCHEM-CRI (a) for present scenario, (b) for pre-industrial scenario.

more rapid than in winter time causing high levels of ozone, thus the production of NO_3 through the reaction of NO_2 and O_3 is increased over the polluted regions of the northern hemisphere (Fig. 4).

The zonal distribution of NO_3 shows the peak at the surface between 30°N and 50°N during J-J-A time. However, two peaks (5–15°N and 20–35°N) and one peak (0–15°N) at the surface in equatorial regions are found during D-J-F time for present and pre-industrial scenarios, respectively. The NO_3 concentrations decrease significantly with altitude (see Fig. 5).

3.4. Evaluation of HO_x recycling

Fig. 6 shows the percentage change in NO_3 between the base and the isoprene sensitivity runs for both present and pre-industrial runs. There is a general increase in NO_3 levels over land whilst a decrease in NO_3 over oceans. NO_3 has increased by up to 80% over land and reduced by up to 40% over the oceans in the surface layer. The highest NO_3 increases (up to about 60% for the present day case and up to 80% for pre-industrial case) are found in J-J-A time over the equatorial regions with high VOC (mostly isoprene) emissions and low NO_x emissions. The highest concentration changes in ozone are over the forested region where the recycling chemistry has the highest effect. The changes in ozone are driven by the redistribution of NO_x which created the highest NO_3 concentration changes in the equatorial regions. There is a small increase in the formation of NO_3 via the reaction of HNO_3 with OH but the large increase in NO_3 is driven by the reduced lifetime of emitted VOCs because of the increase in HO_x concentrations.

3.5. Global impact on NO_3 by inclusion of HO_x recycling

The recycling mechanism employed in STOCHEM-CRI gives results over forested regions that are consistent with the box model

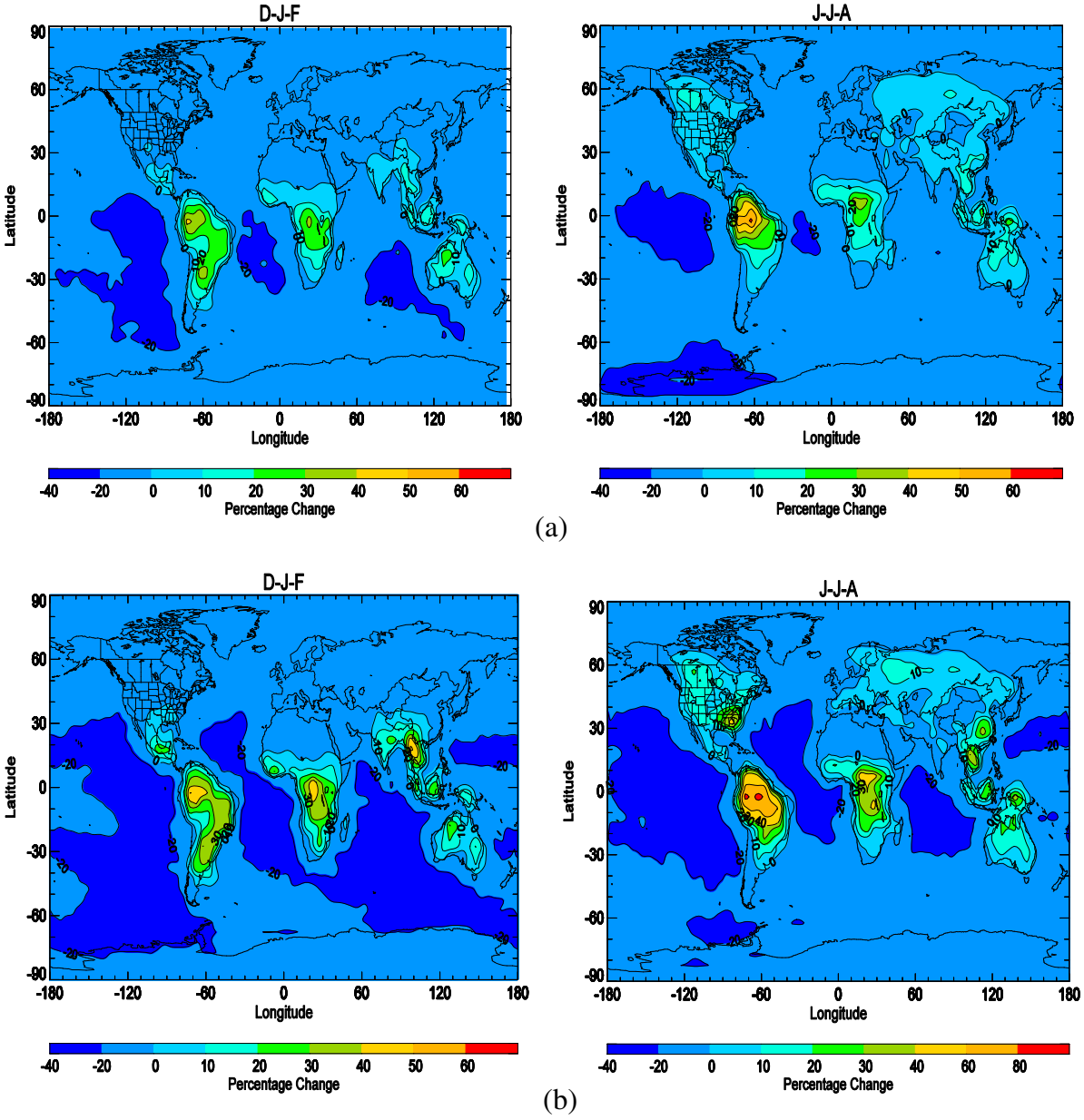

Fig. 6. The percentage changes of NO_3 from HO_x recycling run to base run in December–January–February and June–July–August time for (a) present and (b) pre-industrial scenarios. Note that percentage change (%) = ((ISOP − base)*100)/base.

Table 4
The annual mean global NO_3 and selected species' burden for the base present and pre-industrial run and percentage differences for run ISOP and ISOP1800.

Species	Present			Pre-industrial		
	Base GB (Gg)	ISOP GB (Gg)	% change (ISOP-Base)*100/Base	B1800 GB (Gg)	ISOP1800 GB (Gg)	% change (ISOP1800 − B1800)*100/B1800
NO_3	11.742	11.393	-3.0	4.270	4.047	−5.2
OH	0.246	0.254	3.5	0.271	0.283	4.6
$HOCH_2CHO$	461.317	505.678	9.6	520.533	568.246	9.2
$HOCH_2CO_3$	0.613	0.639	4.3	0.758	0.792	4.5
NRU14O2	1.324	1.341	1.3	0.997	1.036	3.9
NRTN28O2	1.189	1.241	4.4	1.231	1.285	4.4
NRTX28O2	0.666	0.692	3.9	0.576	0.595	3.3

simulations in Archibald et al. (2010a). Table 4 shows the base model global burdens of NO_3 and the percentage changes for HO_x recycling for both present and pre-industrial scenarios. The increased production of OH has led to a global decrease of 3.0% and 5.2% in NO_3 for present and pre-industrial cases, respectively. The inclusion of HO_x recycling leads to greater $HOCH_2CHO$ formation (9.6% for present and 9.2% for pre-industrial). The reduced NO_3 in isoprene HO_x recycling is driven by the increased loss (18.9% for present and 23.3% for pre-industrial) via reaction with $HOCH_2CHO$. The concentration of some peroxy radicals (mainly produced in night) is a balance between faster production via VOC oxidation by NO_3 and faster removal via reaction with NO_3. The isoprene HO_x recycling increased the amount of $HOCH_2CO_3$ (4.3% for present and 4.5% for pre-industrial), NRU14O2 (1.3% for present and 3.9% for pre-industrial), NRTN28O2 (4.4% for both present and pre-industrial), and NRTX28O2 (3.9% for present and 3.3% for pre-industrial) which can also dominate the removal processes of NO_3.

3.6. Pre-industrial vs present scenarios

The maximum concentration changes (up to 15 ppt) and percentage changes (up to 4000%) from pre-industrial to present scenarios for NO_3 are found at the surface between 30°N and 60°N (Fig. 7). The anthropogenic emissions are predominantly between 30°N and 60°N, and therefore, this is where the most significant increases are. The increase in NO_3 over this area since the pre-industrial period is because of increases in NO_x and O_3 levels. This has the effect of reducing the isoprene and terpene concentrations because they are emitted over the forested regions and are predominantly removed by reaction with NO_3 at nighttime.

4. Conclusion

The night-time oxidant, NO_3 is predominantly formed in the troposphere by the reaction of NO_2 and ozone, and therefore, the regional distribution follows the same pattern as ozone and NO_x. The more complex degradation chemistry in CRI v2-R5 leads to a large reduction in the concentration of night-time NO_3. The modeled data of NO_3 for some selected stations showed a general seasonal trend with higher levels in summer and lower levels in the winter. Although there are model uncertainties associated with the chemistry, meteorology, emission scenarios, good agreement between model and measurement data is found suggesting that the STOCHEM-CRI model produces a realistic distribution of NO_3 on global scales throughout the year. The global impact of including HO_x recycling results in an increase of up to 60% in NO_3 concentration over tropical areas because the increased production of OH has shortened the lifetime of VOC leading to increase of NO_3 concentration in the troposphere. In a pre-industrial scenario, the lower NO_x levels make recycling during isoprene oxidation a more favorable pathway. The inclusion of HO_x recycling decreases ozone concentrations which lowers the production of NO_3 in pre-industrial scenarios.

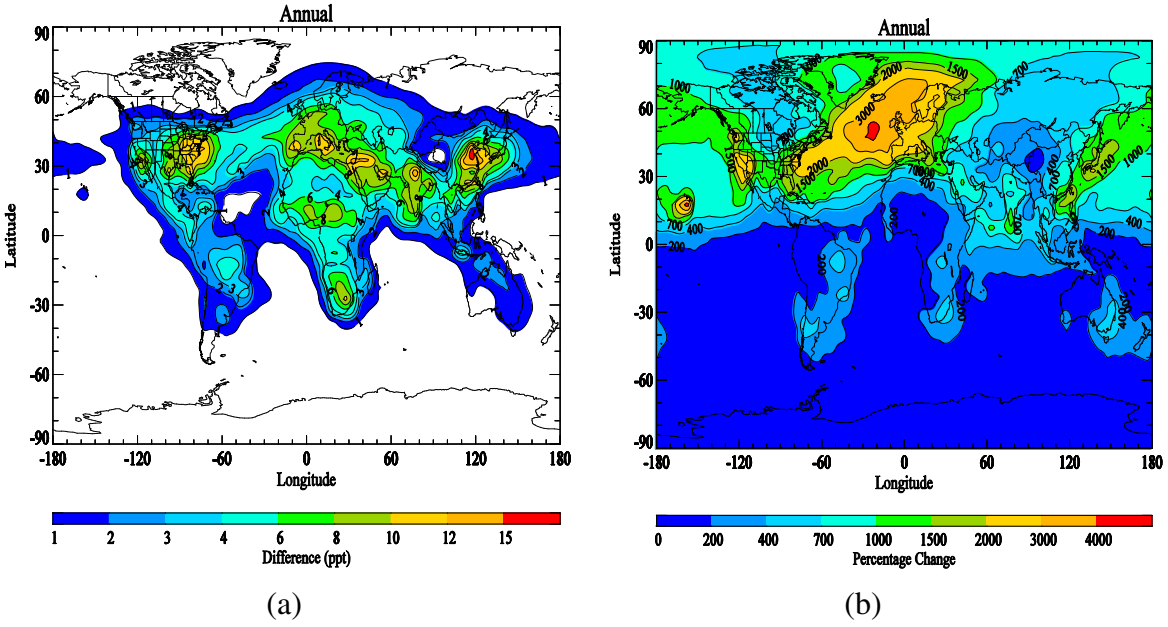

Fig. 7. The surface and annual mean (a) NO_3 mixing ratio difference between present and pre-industrial day, (b) percentage changes from pre-industrial to present day for NO_3. [% = ((Base − B1800)*100)/B1800].

Acknowledgments

ATA thanks GWR and the U.K. Met. Office for funding (studentship), MCC thanks EPSRC for a studentship, DES and CJP thank NERC and Bristol ChemLabS under whose auspices various aspects of this work was funded.

Appendix A. Supplementary data

Supplementary data to this article can be found online at http://dx.doi.org/10.1016/j.atmosres.2015.06.006.

References

Aliwell, S.R., Jones, R.L., 1996. Measurement of atmospheric NO_3, 2. Diurnal variation of stratospheric NO_3 at midlatitude. Geophys. Res. Lett. 23, 2589–2592.
Allan, B.J., Carslaw, N., Coe, H., Burgess, R.A., Plane, J.M.C., 1999. Observations of the nitrate radical in the marine boundary layer. J. Atmos. Chem. 33 (2), 129–154.
Allan, B.J., McFiggans, G., Plane, J.M.C., Coe, H., McFadyen, G.G., 2000. The nitrate radical in the remote marine boundary layer. J. Geophys. Res. 105, 24191–24204.
Andreae, M.O., Merlet, P., 2001. Emission of trace gases and aerosols from biomass burning. Glob. Biogeochem. Cycles 15, 955–966.
Archer-Nicholls, S., Lowe, D., Utembe, S., Allan, J., Zaveri, R.A., Fast, J.D., Hodnebrog, ∅., van der Gon, H.D., McFiggans, G., 2014. Gaseous chemistry and aerosol mechanism developments for version 3.5.1 of the online regional model. WRF-Chem, Geosci. Model Dev. 7, 2557–2579.
Archibald, A.T., Cooke, M.C., Utembe, S.R., Shallcross, D.E., Derwent, R.G., Jenkin, M.E., 2010a. Impacts of mechanistic changes on HO_x formation and recycling in the oxidation of isoprene. Atmos. Chem. Phys. 10, 8097–8118.
Archibald, A.T., Jenkin, M.E., Shallcross, D.E., 2010b. An isoprene mechanism intercomparison. Atmos. Environ. 44 (40), 5356–5364.
Asaf, D., Pedersen, D., Matveev, V., Peleg, M., Kern, C., Zingler, J., Platt, U., Luria, M., 2009. Long-term measurements of NO_3 radical at a semiarid urban site: 1. Extreme concentration events and their oxidation capacity. Environ. Sci. Technol. 43, 9117–9123.
Asaf, D., Tas, E., Pedersen, D., Peleg, M., Luria, M., 2010. Long-term measurements of NO_3 radical at a semiarid urban site: 2. Seasonal trends and loss mechanisms. Environ. Sci. Technol. 44, 5901–5907.
Atkinson, R., 1991. Kinetics and mechanism of the gas-phase reactions of the NO_3 radical with organic compounds. J. Phys. Chem. Ref. Data 20, 459–507.
Atkinson, R., Arey, J., 2003. Atmospheric degradation of volatile organic compounds. Chem. Rev. 103, 4605–4638.
Ball, S.M., Povey, I.M., Norton, E.G., Jones, R.L., 2001. Broad-band cavity ring down spectroscopy of the NO_3 radical. Chem. Phys. Lett. 342, 113–120.
Bertram, T.H., Thornton, J.A., 2009. Toward a general parameterization of N2O5 reactivity on aqueous particles: the competing effects of particle liquid water, nitrate and chloride. Atmos. Chem. Phys. 9, 8351–8363.
Biggs, P., Canosa-Mas, C.E., Fracheboud, J.-M., Shallcross, D.E., Wayne, R.P., 1994. Investigation into the kinetics and mechanism of the reaction of NO_3 with CH_3O_2 at 298 K and 2.5 torr: a potential source of OH in the night-time troposphere? J. Chem. Soc. Faraday Trans. 90, 1205–1210.
Biggs, P., Canosa-Mas, C.E., Fracheboud, J.M., Shallcross, D.E., Wayne, R.P., 1995. Rate constants for the reactions of C_2H_5, C_2H_5O and $C_2H_5O_2$ radicals with NO_3 at 298 K and 2.2 Torr.? J. Chem. Soc. Faraday Trans. 91, 817–825.
Breider, T.J., Chipperfield, M.P., Richards, N.A.D., Carslaw, K.S., Mann, G.W., Spracklen, D.V., 2010. Impact of BrO on dimethylsulfide in the remote marine boundary layer. Geophys. Res. Lett. 37 (2), L02807.
Brown, S.S., Stutz, J., 2012. Nighttime radical observations and chemistry. Chem. Soc. Rev. 41, 6405–6447.
Brown, S.S., Stark, H., Ciciora, S.J., Ravishankara, A.R., 2001. In-situ measurements of atmospheric NO_3 and N_2O_5 via cavity ring-down spectroscopy. Geophys. Res. Lett. 28, 3227–3230.
Brown, S.S., Stark, H., Ryerson, T.B., Ciciora, S.J., McLaughlin, R.J., Ravishankara, A.R., 2002. Simultaneous in situ detection of atmospheric NO_3 and N_2O_5 via cavity ring-down spectroscopy. Rev. Sci. Instrum. 73, 3291–3301.
Brown, S.S., Osthoff, H.D., Stark, H., Dubé, W.P., Ryerson, T.B., Warneke, C., de Gouw, J.A., Wollny, A.G., Parrish, D.D., Fehsenfeld, F.C., Ravishankara, A.R., 2005. Aircraft observations of daytime NO_3 and N_2O_5 and their implications for tropospheric chemistry. J. Photochem. Photobiol. A Chem. 176, 270–278.
Brown, S.S., Ryerson, T.B., Wollny, A.G., Brock, C.A., Peltier, R., Sullivan, A.P., Weber, R.J., Dubé, W.P., Trainer, M., Meagher, J.F., Fehsenfeld, F.C., Ravishankara, A.R., 2006. Variability in nocturnal nitrogen oxide processing and its role in regional air quality. Science 311, 67–70.
Brown, S.S., Dube, W.P., Osthoff, H.D., Stutz, J., Ryerson, T.B., Wollny, A.G., Brock, C.A., Warneke, C., de Gouw, J.A., Atlas, E., Neuman, A., Holloway, J.S., Lerner, B.M., Williams, E.J., Kuster, W.C., Goldan, P.D., Angevine, W.M., Trainer, M., Fehsenfeld, F.C., Ravishankara, A.R., 2007. Vertical profiles in NO_3 and N_2O_5 measured from an aircraft: Results from the NOAA P-3 and surface platforms during the New England Air Quality Study 2004. J. Geophys. Res. 112, D22304.
Canosa-Mas, C.E., King, M.D., Lopez, R., Percival, C.J., Wayne, R.P., Shallcross, D.E., Pyle, J.A., Daele, V., 1996. Is the reaction between $CH_3C(O)O_2$ and NO_3 important in the night-time troposphere? J. Chem. Soc. Faraday Trans. 92 (12), 2211–2222.
Carslaw, N., Plane, J.M.C., Coe, H., 1997. Observations of the nitrate radical in the free troposphere at Izaña de Tenerife. J. Geophys. Res. 102, 10613–10622.
Collins, W.J., Stevenson, D.S., Johnson, C.E., Derwent, R.G., 1997. Tropospheric ozone in a Global-Scale Three-Dimensional Lagrangian Model and its response to NO_x emission controls. J. Atmos. Chem. 26 (3), 223–274.
Crowley, J.N., Burrows, J.P., Moortgat, G.K., Poulet, G., LeBras, G., 1990. Room temperature rate coefficient for the reaction between CH_3O_2 and NO_3. Int. J. Chem. Kinet. 22, 673–681.
Crowley, J.N., Schuster, G., Pouvesle, N., Parchatka, U., Fischer, H., Bonn, B., Bingemer, H., Lelieveld, J., 2010. Nocturnal nitrogen oxides at a rural mountain-site in southwestern Germany. Atmos. Chem. Phys. 10, 2795–2812.
Daele, V., Laverdet, G., LeBras, G., Poulet, G., 1995. Kinetics of the reactions $CH_3O + NO$, $CH_3O + NO_3$, and $CH_3O_2 + NO_3$. J. Phys. Chem. 99, 1470–1477.
Derwent, R.G., Collins, W.J., Jenkin, M.E., Johnson, C.E., Stevenson, D.S., 2003. The global distribution of secondary particulate matter in a 3-D Lagrangian chemistry transport model. J. Atmos. Chem. 44, 57–95.
Fish, D.J., Shallcross, D.E., Jones, R.L., 1999. The vertical distribution of NO_3 in the atmospheric boundary layer. Atmos. Environ. 33, 687–691.
Galmarini, S., Duynkerke, P.G., Vila-Guerau de Arellano, J., 1997. Evolution of nitrogen oxide chemistry in the nocturnal boundary layer. J. Appl. Meteorol. 36, 943–957.
Geyer, A., Alicke, B., Konrad, S., Schmitz, T., Stutz, J., Platt, U., 2001a. Chemistry and oxidation capacity of the nitrate radical in the continental boundary layer near Berlin. J. Geophys. Res. 106 (D8), 8013–8025.
Geyer, A., Ackermann, R., Dubois, R., Lohrmann, B., Müller, T., Platt, U., 2001b. Long term observation of nitrate radicals in the continental boundary layer near Berlin. Atmos. Environ. 35, 3619–3631.
Geyer, A., Alicke, B., Ackermann, R., Martinez, M., Harder, H., Brune, W.H., di Carlo, P., Williams, E., Jobson, T., Hall, S., Shetter, R., Stutz, J., 2003. Direct observations of daytime NO_3: implications for urban boundary layer chemistry. J. Geophys. Res. 108, 4368.
Granier, C., Lamarque, J.F., Mieville, A., Muller, J.F., Olivier, J., Orlando, J., Peters, J., Petron, G., Tyndall, S., Wallens, S., 2005. POET, a database of surface emissions of ozone precursors. http://www.aero.jussieu.fr/project/ACCENT/POET.php.
Hall, I.W., Wayne, R.P., Cox, R.A., Jenkin, M.E., Hayman, G.D., 1988. Kinetics of the reaction of NO_3 with HO_2. J. Phys. Chem. A 92, 5049–5054.
Hallquist, M., Stewart, D.J., Baker, J., Cox, R.A., 2000. Hydrolysis of N_2O_5 on submicron sulphuric acid aerosols. J. Phys. Chem. A 104 (17), 3984–3990.
Heintz, F., Platt, U., Flentje, H., Dubois, R., 1996. Long-term observations of nitrate radicals at the Tor Station, Kap Arkona (Rügen). J. Geophys. Res. 101, 22,891–22,910.
Henze, D.K., Seinfeld, J.H., Ng, N.L., Kroll, J.H., Fu, T.M., Jacob, D.J., Heald, C.L., 2008. Global modeling of secondary organic aerosol formation from aromatic hydrocarbons: high vs low-yield pathways. Atmos. Chem. Phys. 8, 2405–2420.
Houweling, S., Dentener, F., Lelieveld, J., Walter, B., Dlugokencky, E., 2000. The modeling of tropospheric methane: how well can point measurements be reproduced by a global model? J. Geophys. Res. 105, 8981–9002.
Hoyle, C.R., Myhre, G., Berntsen, T.K., Isaksen, I.S., 2009. Anthropogenic influence on SOA and the resulting radiative forcing. Atmos. Chem. Phys. 9, 2715–2728.
Jenkin, M.E., Watson, L.A., Utembe, S.R., Shallcross, D.E., 2008. A Common Representative Intermediate (CRI) mechanism for VOC degradation. Part-1: gas phase mechanism development. Atmos. Environ. 42, 7185–7195.
Kane, S.M., Caloz, F., Leu, M.T., 2001. Heterogeneous uptake of gaseous N_2O_5 by $(NH_4)_2SO_4$, NH_4HSO_4, and H_2SO_4 aerosols. J. Phys. Chem. A 105 (26), 6465–6470.
Khan, M.A.H., Ashfold, M.J., Nickless, G., Martin, D., Watson, L.A., Hamer, P.D., Wayne, R.P., Canosa-Mas, C.E., Shallcross, D.E., 2008. Night-time NO_3 and OH radical concentrations in the United Kingdom inferred from hydrocarbon measurements. Atmos. Sci. Lett. 9, 140–146.
King, M.D., Dick, E.M., Simpson, W.R., 2000. A new method for the atmospheric detection of the nitrate radical (NO_3). Atmos. Environ. 34, 685–688.
Klein Goldewijk, C.G.M., Battjes, J.J., 1997. A hundred year (1890-1990) database for integrated environmental assessments (HYDE, version 1.1). Report no. 422514002. National Institute of Public Health and the Environment (RIVM), Bilthoven, The Netherlands.
Kukui, A.S., Jungkamp, T.P.W., Schindler, R.N., 1995. Aldehyde formation in the reaction of methoxy radicals with NO_3. Ber. Bunsenges. Phys. Chem. 99, 1565–1567.
Lathiere, J., Hauglustaine, D.A., de Noblet-Ducoudre, N., Krinner, G., Folberth, G.A., 2005. Past and future changes in biogenic volatile organic compound emissions simulated with a global dynamic vegetation model. Geophys. Res. Lett. 32 (20), 1–4.
Li, S.W., Liu, W.Q., Xie, P.H., Qin, M., Yang, Y.J., 2012. Observation of nitrate radical in the nocturnal boundary layer during a summer field campaign in Pearl River Delta, China. Terr. Atmos. Ocean. Sci. 23, 39–48.
Matsumoto, J., Kosugi, N., Imai, H., Kajii, Y., 2005. Development of a measurement system for nitrate radical and dinitrogen pentoxide using a thermal conversion/laser-induced fluorescence technique. Rev. Sci. Instrum. 76, 064101.
Matsumoto, J., Imagawa, K., Imai, H., Kosugi, N., Ideguchi, M., Kato, S., Kajii, Y., 2010. Nocturnal sink of NO_x via NO_3 and N_2O_5 in the outflow from a source area in Japan. Atmos. Environ. 40, 6294–6302.
McLaren, R., Wojtal, P., Majonis, D., McCourt, J., Halla, J.D., Brook, J., 2010. NO_3 radical measurements in a polluted marine environment: links to ozone formation. Atmos. Chem. Phys. 10, 4187–4206.
Mellouki, A., Talukdar, R.K., Bopegedera, A.M.R.P., Howard, C.J., 1993. Study of the kinetics of the reactions of NO_3 with HO_2 and OH. Int. J. Chem. Kinet. 25, 25–39.
Mihelcic, D., Klemp, D., Musgen, P., Patz, H.W., Volz-Thomas, A., 1993. Simultaneous measurements of peroxy and nitrate radicals at Schauinsland. J. Atmos. Chem. 16, 313–335.
Mikaloff-Fletcher, S.E., Tans, P.P., Bruhwiler, L.M., Miller, J.B., Heimann, M., 2004. CH_4 sources estimated from atmospheric observations of CH_4 and its $^{13}C/^{12}C$ isotope ratios: 1. Inverse modeling of source processes. Glob. Biogeochem. Cycles 18, GB4004.

Monks, P.S., 2005. Gas-phase radical chemistry in the troposphere. Chem. Soc. Rev. 34, 376–395.
Ng, N.L., Kwan, A.J., Surratt, J.D., Chan, A.W.H., Chhabra, P.S., Soropshian, A., Pye, H.O.T., Crounse, J.D., Wennberg, P.O., Flagan, R.C., Seinfeld, J.H., 2008. Secondary organic aerosol (SOA) formation from reaction of isoprene with nitrate radicals (NO_3). Atmos. Chem. Phys. 8, 4117–4140.
Orlando, J.J., Tyndall, G.S., Moortgat, G.K., Calvert, J.G., 1993. Quantum yields for NO_3 photolysis between 570 and 635 nm. J. Phys. Chem. 97 (42), 10996–11000.
Ouyang, B., McLeod, M.W., Jones, R.L., Bloss, W.J., 2013. NO_3 radical production from the reaction between the Criegee intermediate CH_2OO and NO_2. Phys. Chem. Chem. Phys. 15, 17070–17075.
Penkett, S.A., Burgess, R.A., Coe, H., Coll, I., Hov, Ø., Lindskog, A., Schmidbauerf, N., Solberg, S., Roemer, M., Thijsse, T., Beck, J., Reeves, C.E., 2007. Evidence for large average concentrations of the nitrate radical (NO_3) in Western Europe from the HANSA hydrocarbon database. Atmos. Environ. 41, 3465–3478.
Percival, C.J., Welz, O., Eskola, A.J., Savee, J.D., Osborn, D.L., Topping, D.O., Lowe, D., Utembe, S.R., Bacak, A., McFiggans, G., Cooke, M.C., Xiao, P., Archibald, A.T., Jenkin, M.E., Derwent, Riipinen, I., Mok, D.W., Lee, E.P., Dyke, J.M., Taatjes, C.A., Shallcross, D.E., 2013. Regional and global impacts of Criegee intermediates on atmospheric aerosol nucleation rates. Faraday Discuss. 165, 45–73.
Platt, U., Perner, D., Harris, G.W., Winer, A.M., Pitts, J.M., 1980. Detection of NO_3 in the polluted troposphere by different optical absorption. Geophys. Res. Lett. 7, 89–92.
Platt, U., LeBras, G., Poulet, G., Burrows, J.P., Moortgat, G., 1990. Peroxy radicals from night-time reaction of NO_3 with organic compounds. Nature 348, 147–149.
Platt, U., Alicke, B., Dubois, R., Geyer, A., Hofzumahaus, A., Holland, F., Martinez, M., Mihelcic, D., Klupfer, T., Lohrmann, B., Patz, W., Perner, D., Rohrer, F., Schafer, J., Stutz, J., 2002. Free radicals and fast photochemistry during BERLIOZ. J. Atmos. Chem. 42, 359–394.
Presto, A.A., Donahue, N.M., 2004. Ozonolysis fragment quenching by nitrate formation: the pressure dependence of prompt OH radical formation. J. Phys. Chem. A 108, 9096–9104.
Ray, A., Daele, V., Vassalli, I., Poulet, G., LeBras, G., 1996. J. Phys. Chem. 100, 5737–5744.
Shallcross, D.E., Taatjes, C.A., Percival, C.J., 2014. Criegee intermediates in the indoor environment: new insights. Indoor Air 24 (5), 495–502.
Sommariva, R., Pilling, M.J., Bloss, W.J., Heard, D.E., Lee, J.D., Fleming, Z.L., Monks, P.S., Plane, J.M.C., Saiz-Lopez, A., Ball, S.M., Bitter, M., Jones, R.L., Brough, N., Penkett, S.A., Hopkins, J.R., Lewis, A.C., Read, K.A., 2007. Night time radical chemistry during the NAMBLEX campaign. Atmos. Chem. Phys. 7, 587–598.
Stark, H., Brown, S.S., Goldan, P.D., Aldener, M., Kuster, W.C., Jakoubek, R., Fehsenfeld, F.C., Meagher, J., Bates, T.S., Ravishankara, A.R., 2007. Influence of nitrate radical on the oxidation of dimethyl sulfide in a polluted marine environment. J. Geophys. Res. 112, D10S10.
Stone, D., Evans, M.J., Walker, H., Ingham, T., Vaughan, S., Ouyang, B., Kennedy, O.J., McLeod, M.W., Jones, R.L., Hopkins, J., Punjabi, S., Lidster, R., Hamilton, J.F., Lee, J.D., Lewis, A.C., Carpenter, L.J., Forster, G., Oram, D.E., Reeves, C.E., Bauguitte, S., Morgan, W., Coe, H., Aruffo, E., Dari-Salisburgo, C., Giammaria, F., Di Carlo, P., Heard, D.E., 2014. Radical chemistry at night: comparisons between observed and modelled HO_x, NO_3 and N_2O_5 during the RONOCO project. Atmos. Chem. Phys. 14, 1299–1321.
Stutz, J., Wong, K.W., Lawrence, L., Ziemba, L., Flynn, J.H., Rappengluck, B., Lefer, B., 2010. Nocturnal NO_3 radical chemistry in Houston, TX. Atmos. Environ. 44, 4099–4106.
Taatjes, C.A., Shallcross, D.E., Percival, C.J., 2013. Research frontiers in the chemistry of Criegee Intermediates and tropospheric ozonolysis. Phys. Chem. Chem. Phys. 16, 1704–1718.
Tsigaridis, K., Krol, M., Dentener, F.J., Balkanski, Y., Lathiere, J., Metzger, S., Hauglustaine, D.A., Kanakidou, M., 2006. Change in global aerosol composition since preindustrial times. Atmos. Chem. Phys. 6 (12), 5143–5162.
Utembe, S.R., Watson, L.A., Shallcross, D.E., Jenkin, M.E., 2009. A Common Representative Intermediates (CRI) mechanism for VOC degradation. Part 3: Development of a secondary organic aerosol module. Atmos. Environ. 43 (12), 1982–1990.
Utembe, S.R., Cooke, M.C., Archibald, A.T., Jenkin, M.E., Derwent, R.G., Shallcross, D.E., 2010. Using a reduced Common Representative Intermediates (CRI v2-R5) mechanism to simulate tropospheric ozone in a 3-D Lagrangian chemistry transport model. Atmos. Environ. 13, 1609–1622.
van Aardenne, J., Dentener, J.F., Olivier, J.G.J., Klein Goldewijk, C.G.M., Lelieveld, J., 2001. A $1^o \times 1^o$ resolution dataset of historical anthropogenic trace gas emissions for the period 1890–1990. Glob. Biogeochem. Cycles 15 (4), 909–928.
Vaughan, S., Canosa-Mas, C.E., Pfrang, C., Shallcross, D.E., Watson, L., Wayne, R.P., 2006. Kinetic studies of reactions of the nitrate radical (NO_3) with peroxy radicals (RO_2): an indirect source of OH at night? Phys. Chem. Chem. Phys. 8 (32), 3749–3760.
Vrekoussis, M., Mihalopoulos, N., Gerasopoulos, E., Kanakidou, M., Crutzen, P.J., Lelieveld, J., 2007. Two-years of NO3 radical observations in the boundary layer over the Eastern Mediterranean. Atmos. Chem. Phys. 7, 315–327.
Wang, S., Shi, C., Zhou, B., Zhao, H., Wang, Z., Yang, S., 2013. Observation of NO_3 radicals over Shanghai, China. Atmos. Environ. 70, 401–409.
Wang, X., Wang, T., Yan, C., Tham, Y.J., Xue, L., Xu, Z., Zha, Q., 2014. Large daytime signals of N2O5 and No3 inferred at 52 amu in a TD-CIMS: chemical interference or a real atmospheric phenomenon? Atmos. Meas. Tech. 7, 1–12.
Watson, L.A., Shallcross, D.E., Utembe, S.R., Jenkin, M.E., 2008. A Common Representative Intermediate (CRI) mechanism for VOC degradation. Part 2: gas phase mechanism reduction. Atmos. Environ. 42 (31), 7196–7204.
Wayne, R.P., Barnes, I., Biggs, P., Burrows, J.P., Canosas-Mas, C.E., Hjorth, J., LeBrass, G., Moortgat, G.K., Perner, D., Poulet, G., Restelli, G., Sidebottom, H., 1991. The nitrate radical: physics, chemistry, and the atmosphere. Atmos. Environ. 25A, 1–203.
Welz, O., Savee, J.D., Osborn, D.L., Vasu, S.S., Percival, C.J., Shallcross, D.E., Taatjes, C.A., 2012. Direct kinetic measurements of criegee intermediate (CH_2OO) formed by reaction of CH_2I with O_2. Science 335, 204–207.
Wood, E.C., Wooldridge, P.J., Freese, J.H., Albrecht, T., Cohen, R.C., 2003. Prototype for in situ detection of atmospheric NO_3 and N_2O_5 via laser-induced fluorescence. Environ. Sci. Technol. 37, 5732–5738.
Yvon, S.A., Plane, J.M.C., Nien, C.F., Cooper, D.J., Saltzman, E.S., 1996. Interaction between nitrogen and sulphur cycles in the polluted marine boundary layer. J. Geophys. Res. 101 (D1), 1379–1386.